A Bound on Ekman Pumping

de Roode, Stephan R.; Siebesma, A. Pier

DOI
10.1029/2019MS001976

Publication date
2020

Document Version
Final published version

Published in
Journal of Advances in Modeling Earth Systems

Citation (APA)
de Roode, S. R., & Siebesma, A. P. (2020). A Bound on Ekman Pumping. *Journal of Advances in Modeling Earth Systems*, *12*(3), Article e2019MS001976. https://doi.org/10.1029/2019MS001976

JAMES | Journal of Advances in Modeling Earth Systems

RESEARCH ARTICLE
10.1029/2019MS001976

Key Point:
- The large-scale vertical velocity caused by boundary layer turbulent friction has a maximum value

Correspondence to:
S. R. de Roode,
s.r.deroode@tudelft.nl

Citation:
de Roode, S. R., & Siebesma, A. P. (2020). A bound on Ekman pumping. *Journal of Advances in Modeling Earth Systems*, *12*, e2019MS001976. https://doi.org/10.1029/2019MS001976

Received 11 DEC 2019
Accepted 17 FEB 2020
Accepted article online 19 FEB 2020

A Bound on Ekman Pumping

Stephan R. de Roode[1] **and A. Pier Siebesma**[1,2]

[1]Faculty of Civil Engineering and Geosciences, Department of Geoscience and Remote Sensing, Delft University of Technology, Delft, Netherlands, [2]KNMI, De Bilt, Netherlands

Abstract Momentum transport by boundary layer turbulence causes a weak synoptic-scale vertical motion. The classical textbook solution for the strength of this Ekman pumping depends on the curl of the surface momentum flux. A new solution for Ekman pumping is derived in terms of the curl of the geostrophic wind and a term that depends in a nontrivial way on the vertical profile of the turbulent momentum flux. The solution is confined to a boundary layer regime that is vertically well mixed and horizontally homogeneous. The momentum flux is computed from a commonly used bulk surface drag formula and a flux jump relation to capture the entrainment flux of momentum at the top of the boundary layer. It is found that the strength of Ekman pumping is bounded. The weakening of Ekman pumping for enhanced turbulent surface friction can be explained from the fact that it will reduce the magnitude of the horizontal wind. It is demonstrated that entrainment of momentum across the top of the boundary layer tends to diminish the large-scale divergence of the wind. As momentum transport is parameterized in large-scale models, the analysis is relevant for the understanding and interpretation of the evolution of synoptic-scale vertical motions as predicted by such models.

Plain Language Summary Turbulence acts as a friction to the wind. This drives a net flow of air from high to low pressure. The resulting accumulation of mass drives an upward vertical motion in a low-pressure system and vice versa in a high-pressure system. This study shows that the vertical velocity caused by turbulent friction has a maximum value.

1. Introduction

Geostrophic flow is at the heart of dynamical meteorology. It elucidates why in a synoptic system of (low) high pressure on the Northern Hemisphere the wind vector is tangent to the isobars in a (counter)clockwise direction. However, this theoretical wind structure is fully two-dimensional with a zero vertical velocity component. In fact, the presence of synoptic-scale vertical motion actually requires the consideration of turbulent boundary layer eddies that act as a drag on the mean flow. As depicted schematically in Figure 1, this friction effect gives rise to a net horizontal transport of air from high to low pressure. The resulting accumulation of mass drives a large-scale upward vertical velocity in a low-pressure system and vice versa in a high-pressure system. Because the magnitude of the turbulent friction controls the strength of the cross-isobaric flow (Svensson & Holtslag, 2009), it impacts the evolution of (anti) cyclones at synoptic scales (Sandu et al., 2013).

Although the characteristic synoptical-scale vertical velocity is small, typically on the order of cm s^{-1}, its effect on the evolution of the boundary layer cannot be neglected. Large-scale subsidence tends to advect the boundary layer top downward (Lilly, 1968), which has a strong impact on, for example, the concentration of air pollution in the atmospheric boundary layer (Seibert et al., 2000), the evolution of stratocumulus (Van der Dussen et al., 2016; Zhang et al., 2009), and Arctic mixed-phase stratocumulus (Young et al., 2018). On the other hand, convergence of air leads to an upward motion of air. Saturation of air, and subsequently clouds, may develop as rising air cools down adiabatically. The generation of precipitation in such a system will be strongly controlled by the large-scale convergence (Back & Bretherton, 2009) .

Various efforts have been made to assess the large-scale subsidence from field observations of horizontal wind and with the use of the equation for conservation of mass,

$$\frac{\partial U}{\partial x} + \frac{\partial V}{\partial y} + \frac{\partial W}{\partial z} = 0, \tag{1}$$

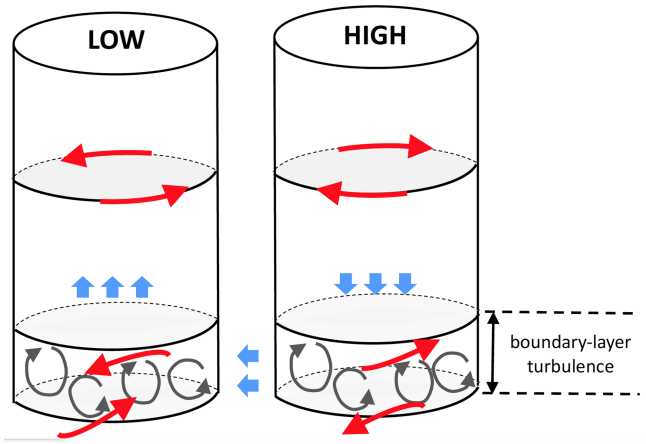

Figure 1. A schematic representation of Ekman pumping in a synoptic low- and high-pressure system (adapted from Marshall & Plumb, 2016). Boundary layer eddies cause a cross-isobaric flow in which a net transport of air from high to low pressure occurs. This leads to a convergence of air in the low-pressure system and a subsequent large-scale ascending motion. In the high-pressure system large-scale subsidence is induced.

with U, V, W the east-west (x), north-south (y), and vertical (z) components of the wind vector, respectively. The mean vertical velocity is controlled by the large-scale divergence of horizontal wind,

$$D \equiv \left(\frac{\partial U}{\partial x} + \frac{\partial V}{\partial y} \right) = -\frac{\partial W}{\partial z}. \tag{2}$$

This diagnostic expression proved useful to study the diurnal cycle of D from radiosondes that were launched during the Atlantic Stratocumulus Transition EXperiment (Ciesielski et al., 1999). Lenschow et al. (2007) studied aircraft measurements of the horizontal wind field collected from circular legs flown during the Second Dynamics and Chemistry of Marine Stratocumulus experiment, and they concluded that this measurement strategy is not suitable to diagnose D as it yields unacceptable large errors. By contrast, from a careful analysis of observations from dropsondes that were released from an aircraft that flew along circular patterns over the tropical Atlantic near Barbados, Bony et al. (2017) demonstrated that this strategy can actually be rather well used to determine D with a sufficient accuracy.

A well-known and frequently used solution for the mean vertical motion depends on the curl of the surface momentum flux (Beare, 2007). In this note a new diagnostic equation for the large-scale divergence of the horizontal wind D in terms of the strength of a nondimensional turbulent boundary layer friction factor and entrainment of momentum across the top of the boundary layer will be derived. It will be demonstrated that this solution predicts a maximum value for the large-scale divergence of the horizontal wind.

2. Theory

The dependency of the large-scale vertical velocity on the momentum flux profile can be readily obtained from the conservation equations for momentum and mass. The main goal of this note is to study the effect of boundary layer friction on Ekman pumping. To this end we will consider an idealized steady-state, horizontally homogeneous and vertically well-mixed boundary layer forced by a constant geostrophic wind. The momentum flux will be specified in terms of a bulk surface friction factor and an entrainment velocity at the top of the boundary layer.

The mixed-layer model framework originally developed by Stevens et al. (2002) is depicted schematically in Figure 2. The horizontal wind is constant with height in the boundary layer. This approximation holds rather well for convectively driven atmospheric boundary layers. Further support for the use of this model is given by Back and Bretherton (2009), who showed that it can skilfully reproduce observed surface winds and convergence over the tropical oceans.

2.1. Governing Equations

The horizontal momentum equations read

$$\frac{\mathrm{d}U}{\mathrm{d}t} = fV - \frac{1}{\rho}\frac{\partial P}{\partial x} - \frac{\partial \overline{uw}}{\partial z}, \tag{3}$$

$$\frac{\mathrm{d}V}{\mathrm{d}t} = -fU - \frac{1}{\rho}\frac{\partial P}{\partial y} - \frac{\partial \overline{vw}}{\partial z}, \tag{4}$$

with P the pressure, f the Coriolis parameter, and $\overline{uw}$ and $\overline{vw}$ the Reynolds averaged momentum fluxes. Due to our assumption of horizontal homogeneity, the mean horizontal advection terms vanish. Mean vertical advection of momentum is 0 as in the boundary layer the wind is assumed to be constant with height. Last, we will use a constant value for the density of air ρ.

In the absence of turbulence a geostrophic balance is maintained by the Coriolis and the pressure gradient forces,

$$U = U_\mathrm{g} \equiv -\frac{1}{\rho f}\frac{\partial P}{\partial y} \quad , \quad V = V_\mathrm{g} \equiv \frac{1}{\rho f}\frac{\partial P}{\partial x}, \tag{5}$$

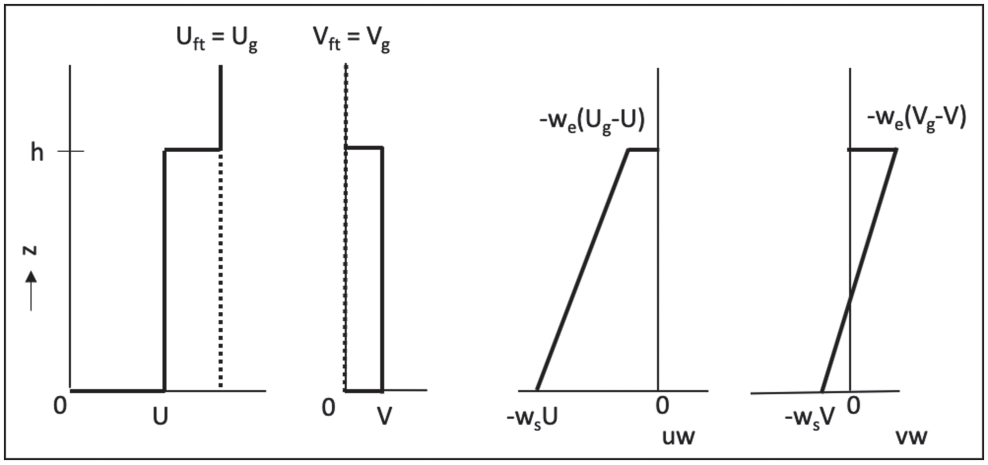

Figure 2. A schematic representation of the vertical profiles of the steady-state horizontal wind components and their vertical turbulent fluxes (thick black lines) for a forcing $U_g > 0$ (indicated by the black dotted vertical line) and $V_g = 0$. The momentum fluxes at the surface and at the top of the boundary layer are computed with bulk formulae.

with U_g and V_g defining the geostrophic wind velocity components. The fact that a purely geostrophic flow does not support any mean vertical motion can be derived from a substitution of the geostrophic solution equation (5) in equation (2) which gives $D = 0$.

The importance of turbulence on the vertical motion becomes clear after a differentiation of equations (3) and (4) with respect to y and x, respectively, and the use of these expressions in equation (2),

$$-\frac{\partial}{\partial z}\left[fW - \frac{\partial \overline{uw}}{\partial y} + \frac{\partial \overline{vw}}{\partial x}\right] = 0. \tag{6}$$

Here we reversed the order of differentiation in the pressure and momentum flux terms. The latitudinal variation of the Coriolis parameter $\partial f/\partial y$ will be ignored. The vertical gradient of W has entered equation (6) by the use of the continuity equation (1). A vertical integration from the surface (indicated by the subscript "sfc") upward to the height h^+, which is just above the boundary layer where turbulence vanishes, shows that the vertical velocity depends on the curl of the surface momentum fluxes (Beare, 2007),

$$W|_{h^+} = \frac{1}{f}\left(\frac{\partial \overline{uw}_{\mathrm{sfc}}}{\partial y} - \frac{\partial \overline{vw}_{\mathrm{sfc}}}{\partial x}\right), \tag{7}$$

with $W = 0$ at the ground surface. The vertical velocity that is driven by surface momentum fluxes is called Ekman pumping after the Swedish oceanographer who was the first to derive an analytical solution for wind-driven horizontal transport in the ocean. Ekman's solution for ocean flow is widely used as a powerful diagnostic tool that relates the strength of Ekman pumping in the ocean to the curl of the wind stress exerted at the Ocean's surface. Note that equation (7) ignores the effect of entrainment fluxes at the top of the boundary layer. To further explore the role of the momentum fluxes on Ekman pumping, we will now apply parameterizations for their values at the surface and at the top of the boundary layer due to entrainment.

2.2. Parameterization of the Momentum Flux

The surface momentum fluxes can be expressed by the following bulk formula

$$(\overline{uw}_{\mathrm{sfc}}, \overline{vw}_{\mathrm{sfc}}) = -C_{\mathrm{d}} U_{\mathrm{spd}}(U, V), \tag{8}$$

with U_{spd} the wind speed,

$$U_{\mathrm{spd}} = \sqrt{U^2 + V^2}. \tag{9}$$

The factor C_{d} is turbulent drag coefficient that depends on the vertical stability and the roughness length (Schröter et al., 2013). Because the magnitude of U_{spd} is controlled by the surface drag coefficient C_{d}, the parameterization of the surface momentum flux has introduced a nonlinearity in the system. To avoid

this additional complexity, the formulation of the surface momentum flux may be further simplified by introducing a linearized friction coefficient (Back & Bretherton, 2009),

$$w_{\mathrm{sfc}} = C_{\mathrm{d}} U_{\mathrm{spd}}. \tag{10}$$

This factor is sometimes referred to as a surface ventilation velocity.

The flux at the top of the boundary layer, denoted by h, can be expressed by the "flux jump" relation in a similar fashion (Lilly, 1968),

$$\overline{uw}_h = -w_{\mathrm{e}}(U_{\mathrm{ft}} - U) \quad , \quad \overline{vw}_h = -w_{\mathrm{e}}(V_{\mathrm{ft}} - V), \tag{11}$$

with w_{e} the entrainment velocity, and the subscript "ft" represents the value of free tropospheric value of the wind just above the boundary layer. In the remainder we will assume that the wind in the free troposphere is in a geostrophic balance, $(U_{\mathrm{ft}}, V_{\mathrm{ft}}) = (U_{\mathrm{g}}, V_{\mathrm{g}})$. Because both the actual and geostrophic winds are assumed to be constant with height in the boundary layer, the condition of a steady state requires that the momentum flux must vary linearly with height in order to balance their net force, which allows to express the vertical change of the momentum fluxes as follows,

$$\frac{\partial \overline{uw}}{\partial z} = \frac{-w_{\mathrm{e}}(U_{\mathrm{g}} - U) + w_{\mathrm{sfc}} U}{h} \quad , \quad \frac{\partial \overline{vw}}{\partial z} = \frac{-w_{\mathrm{e}}(V_{\mathrm{g}} - V) + w_{\mathrm{sfc}} V}{h}, \tag{12}$$

to give the following momentum balance equations,

$$\begin{aligned} V - V_{\mathrm{g}} + k_{\mathrm{top}} U_{\mathrm{g}} - (k_{\mathrm{sfc}} + k_{\mathrm{top}}) U = 0, \\ -U + U_{\mathrm{g}} + k_{\mathrm{top}} V_{\mathrm{g}} - (k_{\mathrm{sfc}} + k_{\mathrm{top}}) V = 0. \end{aligned} \tag{13}$$

Here we introduced the nondimensional factors,

$$k_{\mathrm{sfc}} = \frac{w_{\mathrm{sfc}}}{fh} \quad , \quad k_{\mathrm{top}} = \frac{w_{\mathrm{e}}}{fh}. \tag{14}$$

The factor k_{sfc} may be interpreted as a turbulent Ekman number as it compares the importance of surface ("viscous") friction relative to the Coriolis force.

The use of the factor w_{sfc} enables us to solve U and V analytically from equation (13). In the next section we will effectively apply this strategy. This is motivated by the fact that the analytical solutions for the boundary layer wind, and more specifically their dependency on the nondimensional factors k_{sfc} and k_{top}, will demonstrate some important general behavior of Ekman pumping. However, in section 3.3 we will discuss an example that is based on numerical solutions of the momentum equations for a prescribed value of the bulk surface friction C_{d}.

3. Analytical Solutions for the Large-Scale Divergence and Subsidence

Here we present and discuss the analytical solutions for the large-scale flow that follow from the steady-state linearized momentum equations (13).

3.1. Analytical Steady-State Solutions

The solutions for the horizontal wind can be expressed in terms of the geostrophic wind,

$$\begin{aligned} U &= \frac{1 + k_{\mathrm{top}}(k_{\mathrm{sfc}} + k_{\mathrm{top}})}{1 + (k_{\mathrm{sfc}} + k_{\mathrm{top}})^2} U_{\mathrm{g}} - \frac{k_{\mathrm{sfc}}}{1 + (k_{\mathrm{sfc}} + k_{\mathrm{top}})^2} V_{\mathrm{g}}, \\ V &= \frac{1 + k_{\mathrm{top}}(k_{\mathrm{sfc}} + k_{\mathrm{top}})}{1 + (k_{\mathrm{sfc}} + k_{\mathrm{top}})^2} V_{\mathrm{g}} + \frac{k_{\mathrm{sfc}}}{1 + (k_{\mathrm{sfc}} + k_{\mathrm{top}})^2} U_{\mathrm{g}}. \end{aligned} \tag{15}$$

The divergence of the horizontal wind field can be obtained with aid of equation (2),

$$D = F(k_{\mathrm{sfc}}, k_{\mathrm{top}}) \left(\frac{\partial U_{\mathrm{g}}}{\partial y} - \frac{\partial V_{\mathrm{g}}}{\partial x} \right) = -F(k_{\mathrm{sfc}}, k_{\mathrm{top}}) \frac{\nabla^2 P}{\rho f}, \tag{16}$$

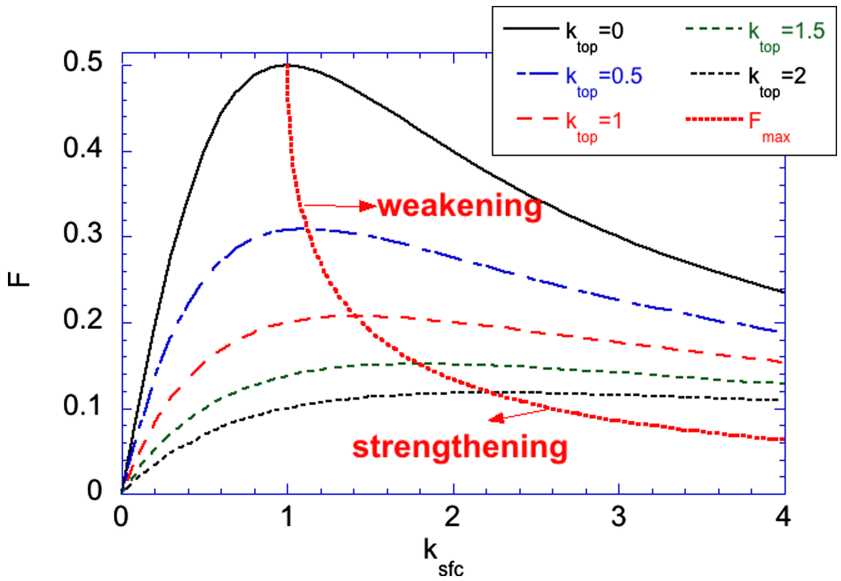

Figure 3. The factor F as a function of the nondimensional surface friction (k_{sfc}) and entrainment (k_{top}) factors as defined by equation (17). The red dotted line connects the maximum values for the function F. The regime left of the red dotted line is indicated by "strengthening," which means that the large-scale divergence D increases for increasing k_{sfc}. In the weakening regime, D will decrease for increasing k_{sfc}. The line styles are according to the legend.

where we introduced the function

$$F(k_{\mathrm{sfc}}, k_{\mathrm{top}}) = \frac{k_{\mathrm{sfc}}}{1 + (k_{\mathrm{sfc}} + k_{\mathrm{top}})^2}, \tag{17}$$

and ∇ indicates the Laplacian operator in the horizontal directions. The function F is also present in the solution for the large-scale vertical velocity, whose magnitude at the top of the boundary layer can be readily obtained from a vertical integration of D,

$$w|_h = -F(k_{\mathrm{sfc}}, k_{\mathrm{top}}) \left(\frac{\partial U_{\mathrm{g}}}{\partial y} - \frac{\partial V_{\mathrm{g}}}{\partial x} \right) h, \tag{18}$$

where we assumed that the value of D is constant within the boundary layer, which is not an uncommon assumption for vertically well-mixed boundary layers (Stevens, 2006).

3.2. Interpretation

The solutions for the mean vertical velocity (7) and (18) differ in the sense that the former depends on the curl of the surface momentum flux, whereas the new solution equation (18) depends on the curl of the geostrophic wind or, alternatively, on the Laplacian of the pressure field. One might be tempted to hypothesize that a larger surface friction will yield a stronger Ekman pumping from the premise that more surface friction will cause an enhancement of the surface momentum flux. We will now argue that k_{sfc} puts a bound on the strength of Ekman pumping, a condition that cannot be inferred directly from equation (7).

3.2.1. Surface Friction Effect, No Entrainment ($k_{\mathrm{top}} = 0$)

Let us inspect the function F shown in Figure 3. For a frictionless flow, $k_{\mathrm{sfc}} = k_{\mathrm{top}} = 0$, we recover the solutions of a geostrophic balance (5), and consequently there will be no large-scale divergence since $F = 0$. For $k_{\mathrm{sfc}} > 0$ we find that $V > 0$, which indicates that cross-isobaric flow occurs. The presence of this ageostrophic wind component results in the large-scale divergence (or convergence) of the flow that, in turn, drives the large-scale vertical motions. If the surface friction goes to infinity, or equivalently, $k_{\mathrm{sfc}} \to \infty$, then $F \to 0$. In this limit surface friction damps the horizontal wind to 0, and subsequently the large-scale divergence $D \to 0$. This leads to the key conclusion that the effect of surface friction on the large-scale vertical velocity is bounded. Equation (17) predicts that the large-scale divergence is maximum with $F = 1$ for $k_{\mathrm{sfc}} = 1$ and zero entrainment, $k_{\mathrm{top}} = 0$. According to equation (15) this solution corresponds to $U = V = \frac{1}{2} U_{\mathrm{g}}$, and since the angle of the actual wind with the geostrophic wind is given by $\tan \alpha = V/U$, we find this so-called ageostrophic angle to be equal to $\alpha = 45°$.

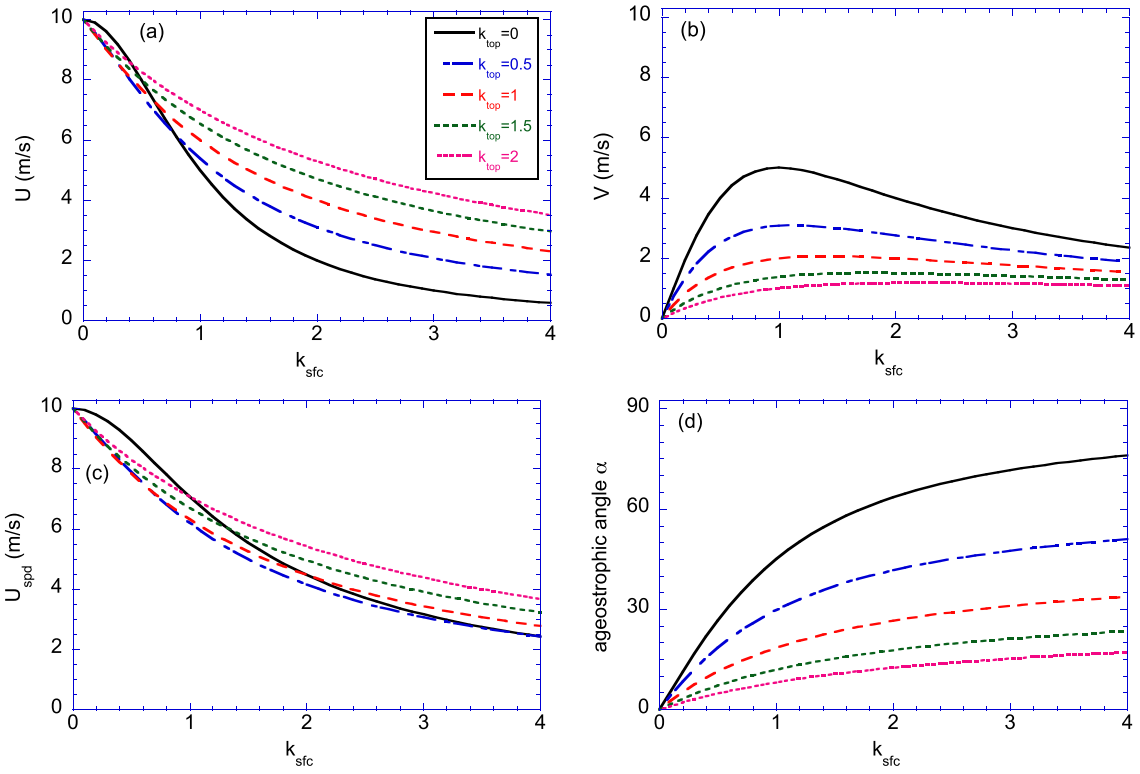

Figure 4. The wind component (a) U, (b) V, (c) wind speed U_{spd}, and (d) the ageostrophic angle α as a function of the nondimensional surface friction (k_{sfc}) and entrainment (k_{top}) factors as defined by equation (17) for $U_{\mathrm{g}} = 10$ m s^{-1} and $V_{\mathrm{g}} = 0$. The line styles are according to the legend.

3.2.2. Combined Surface Friction and Entrainment

Before discussing the large-scale divergence let us first discuss the solutions for the horizontal wind according to equation (15), which show that in the presence of turbulence the steady-state wind speed becomes

$$U_{\mathrm{spd}}{}^2 = \frac{1 + k_{\mathrm{top}}{}^2}{1 + (k_{\mathrm{sfc}} + k_{\mathrm{top}})^2}(U_{\mathrm{g}}{}^2 + V_{\mathrm{g}}{}^2) \leq |\vec{U}_{\mathrm{g}}|^2. \tag{19}$$

Surface friction and entrainment appear to have opposing effects on the wind speed. This can be seen from the limit $k_{\mathrm{sfc}} \to \infty$ which yields a zero wind speed. By contrast, for strong entrainment the free tropospheric wind speed is imposed on the boundary layer, as for $k_{\mathrm{top}} \to \infty$ we find $U_{\mathrm{spd}} \to |\vec{U}_{\mathrm{g}}|$.

Figure 4 shows examples of U, V, U_{spd}, and the ageostrophic angle α for a forcing $U_{\mathrm{g}} = 10$ m s^{-1} and $V_{\mathrm{g}} = 0$. While V tends to become smaller with increasing entrainment velocity, we notice a more delicate dependency of U on entrainment in the sense that for small (large) k_{sfc}, U tends to decrease (increase) for increasing entrainment velocity. This results in a wind speed U_{spd} that tends to diminish for increasing entrainment in the regime $k_{\mathrm{sfc}} < 2/k_{\mathrm{top}}$. Stevens et al. (2002) explains that this is caused by an asymmetry in the entrainment flux. Figure 5 illustrates that entrainment tends to enhance the momentum fluxes at the top of the boundary layer which results, however, in opposing effects on the vertical gradients of $\overline{uw}$ and $\overline{vw}$. If the vertical slope of $\overline{vw}$ is enhanced by a larger entrainment velocity, there will be a stronger damping acting on V by turbulent friction, which results in a smaller steady-state value of V, in accord with the results displayed in Figure 4. As a consequence, the forcing term fV that is present in the budget equation (3) for U is also reduced, and to achieve a steady state, the vertical slope of $\overline{uw}$ has to diminish. An increase in the entrainment velocity can already partly support this, but if this does not yield the requested total change in the vertical gradient of $\overline{uw}$, a balance can be achieved only if U is decreased as well.

An important consequence of the presence of entrainment is that it tends to diminish the large-scale divergence (see Figure 3). Moreover, the maximum value of F is shifted toward larger values of k_{sfc}. This can be

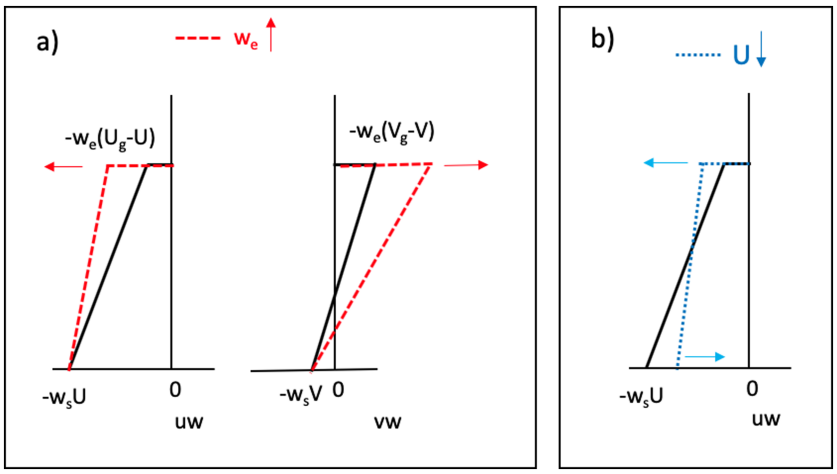

Figure 5. A schematic representation of the effect of (a) an increase in the entrainment velocity (red dashed lines) w_e and (b) a decrease of the horizontal wind component U (blue dotted line) on the momentum flux profiles. The black lines indicate the momentum flux profiles belonging to a steady-state solution for a forcing $U_g > 0$ and $V_g = 0$ as shown in Figure 2. An increase in entrainment causes a larger slope of $\overline{vw}$ (stronger effect of turbulent friction) but a smaller slope of $\overline{uw}$ (smaller effect of turbulent friction).

derived by setting the derivative of the function F with respect to k_{sfc} to 0 to give

$$k_{sfc} = \sqrt{1 + {k_{top}}^2}. \tag{20}$$

3.3. A Numerical Example for a Case With a Prescribed Bulk Surface Drag Coefficient C_d

As a practical illustration of the theory we took the reference case of Stevens et al. (2002), with $h = 500$ m, $w_e = 1$ cm s^{-1}, $U_g = 6$ m s^{-1}. Furthermore C_d is set to 0.0011 which is a typical value over the tropical oceans. However, noting that the relevant parameters k_{sfc} and k_{top} do both depend on reciprocal of the Coriolis parameter, we have computed results up to a latitude of 90°. The sensitivity of the results on the entrainment is addressed by setting w_e to 0. Because U_{spd} depends on the prescribed value of C_d, the solutions shown in Figure 6 were computed numerically, and as a consequence the bulk surface friction factor k_{sfc}, that is now diagnosed from the resulting wind speed according to $k_{sfc} = C_d U_{spd}/hf$, differs for the two cases shown. Except for a narrow band near the tropics, where k_{sfc} exceeds unity, entrainment tends to diminish the wind speed. The wind speed tends to approach the (absolute) value of the geostrophic wind toward higher latitudes. This can be explained from the bulk surface friction factor k_{sfc} whose magnitude diminishes away from the equator. The effect of entrainment on Ekman pumping is evident from the resulting shape of the function F which in the tropical regime is diminished by more than a factor of about 2 with respect to the case without entrainment. In conclusion, the findings suggest that maximum values for the function F are most likely to be expected at low latitudes.

3.4. Discussion

Sandu et al. (2013) evaluated the effect of a less diffusive parameterization for turbulent transport in stably stratified boundary layers in the European Centre for Medium-Range Weather Forecasts model and confirmed that the strength of turbulence diffusion affects the large-scale flow by modulating the strength of synoptic-scale systems. Moreover, they found that the model improved the representation of high-pressure systems, but the storm track region in the Southern Hemisphere was less well captured. Our analysis suggests that the question as to which a change in the parameterization of turbulence in a large-scale weather forecast model leads to either a strengthening or a weakening effect on the evolution of synoptic-scale systems depends on the factors k_{sfc} and k_{top} in a nontrivial way.

It should be noted that the boundary layer depth itself is controlled by the strength of turbulence. For example, the enhancement of turbulent diffusion in stable conditions, used to improve the representation of large-scale synoptic systems, leads not only to larger momentum fluxes but also to deeper boundary layers (Sandu et al., 2013; Svensson & Holtslag, 2009). For the case studied here, a larger entrainment rate will cause a deeper boundary layer, which according to equation (18) will enhance Ekman pumping since

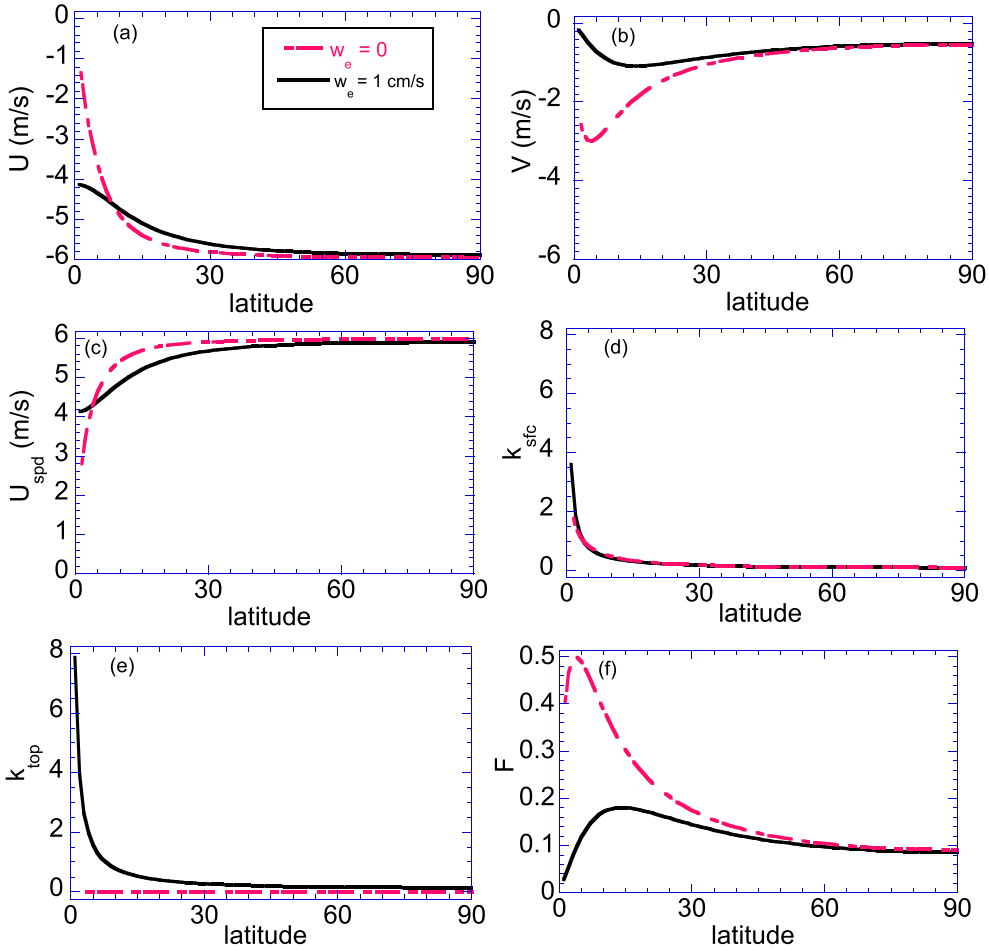

Figure 6. Numerical solutions for the wind velocity (a) U, (b) V, (c) the wind speed U_{spd}, (d) the nondimensional surface friction factor k_{sfc}, (e) the entrainment factor k_{top}, and (f) the function F as a function of the latitude. The forcing conditions were taken from Stevens et al. (2002), $C_{\mathrm{d}} = 0.00111$, $U_{\mathrm{g}} = -6$ m s^{-1}, $h = 500$ m. The results for the wind as obtained for an entrainment velocity of 1 cm s^{-1} are identical to their Figure 1, and the zero entrainment case is added here to illustrate its impact on the wind. The line styles are according to the legend.

cross-isobaric flow will take place over a deeper layer depth h. However, entrainment has an opposing impact on Ekman pumping via its control on the function F. In particular, if the modeled entrainment is too large, the function F will become smaller as shown in Figure 3 . This suggests that a bias in the entrainment in convective well-mixed boundary layers may yield only a limited impact on Ekman pumping.

4. Conclusion

The present study discusses the effect of boundary layer turbulence on the magnitude of the large-scale vertical velocity. In particular, a vertically well-mixed and horizontally homogeneous structure of the boundary layer is assumed. We confine our analysis to steady-state conditions, and we use bulk parameterizations following the mixed-layer model for wind as used in Stevens et al. (2002). We present new diagnostic relations for the large-scale divergence of horizontal wind (D) and the large-scale vertical velocity.

In the absence of entrainment a maximum value for the large-scale divergence D is found if the nondimensional surface friction factor k_{sfc} is equal to unity, a value which corresponds to a situation in which the actual wind has a cross-isobaric (ageostrophic) angle of 45°. The factor k_{sfc} can be thought of as an Ekman number that weighs the importance of the turbulent surface momentum flux relative to the force due to planetary rotation. A maximum value of Ekman pumping can be explained from the following notion. For a purely frictionless geostrophic flow the large-scale divergence of horizontal wind $D = 0$, and consequently there will be no Ekman pumping. The presence of surface friction acts as a drag on the flow that generates

an ageostrophic flow component giving $D \neq 0$, which, in turn, drives a small large-scale velocity. However, in the limit of infinite turbulent surface friction the horizontal wind will tend to 0, and likewise $D = 0$. This reasoning suggests a maximum effect of turbulent surface friction on the magnitude of D, which is quantified in this study. More precisely, D is found to depend on the curl of the geostrophic wind, in addition to a function F that depends on the nondimensional factors related to surface friction and entrainment. It is found that entrainment tends to diminish the large-scale divergence.

The findings reported in this note might be useful to fine-tune parameterizations in global models such as explored in the study by Sandu et al. (2013) and including the ones which apply an explicit formulation of turbulent form drag due to subgrid orography (Beljaars et al., 2004) or to better understand the impact of the parameterization of the bulk drag coefficient C_d on the model outcome (Foreman & Emeis, 2010; Moon et al., 2007). However, our study is restricted to vertically well-mixed layers, a condition that is not applicable to the nocturnal stable boundary layer whose structure exhibits strong vertical gradients.

In the context of the present analysis it is worthwhile to mention some relevant studies on Ekman pumping based on height-dependent solutions for the wind by Wu and Blumen (1982) and Tan (2001). Wu and Blumen derived analytical solutions for the boundary layer wind profile for nonstationary conditions. They maintained the advective transport term in the momentum equation, and they parameterized the momentum flux with a downgradient diffusion approach. Their solution is a modified Ekman spiral, a solution that closely mimics the one that is frequently observed for stable boundary layers, with the wind direction and wind speed depending on the magnitude of the constant eddy viscosity. Tan (2001) investigated the role of a height-dependent eddy viscosity and a baroclinic pressure field on Ekman pumping from an analysis of an approximate solution for the wind. Tan concluded that a variable eddy viscosity and inertial acceleration have an important role in the divergence in the boundary layer and the subsequent Ekman pumping strength. A similar analysis might be performed for a clear convective boundary layer regime. For example, Stevens et al. (2002) presented height-dependent wind profiles as obtained with a turbulent diffusion parameterization.

Acknowledgments
We thank one anonymous reviewer and Dr. Anton Beljaars for some critical yet constructive comments which motivated us to perform the analysis from a mixed-layer framework including entrainment. We also thank Drs. Bert Holtslag, Harm Jonker, and Bas van de Wiel for interesting discussions. No model data were used in this study.

References

Back, L. E., & Bretherton, C. S. (2009). On the relationship between SST gradients, boundary layer winds, and convergence over the tropical oceans. *Journal of Climate*, *22*(15), 4182–4196.

Beare, R. J. (2007). Boundary layer mechanisms in extratropical cyclones. *Quarterly Journal of the Royal Meteorological Society*, *133*(623), 503–515.

Beljaars, A. C., Brown, A. R., & Wood, N. (2004). A new parametrization of turbulent orographic form drag. *Quarterly Journal of the Royal Meteorological Society*, *130*(599), 1327–1347.

Bony, S., Stevens, B., Ament, F., Bigorre, S., Chazette, P., Crewell, S., et al. (2017). EUREC 4A: A field campaign to elucidate the couplings between clouds, convection and circulation. *Surveys in Geophysics*, *38*(6), 1529–1568. https://doi.org/10.1007/s10712-017-9428-0

Ciesielski, P. E., Schubert, W. H., & Johnson, R. H. (1999). Large-scale heat and moisture budgets over the ASTEX region. *Journal of the Atmospheric Sciences*, *56*(18), 3241–3261.

Foreman, R. J., & Emeis, S. (2010). Revisiting the definition of the drag coefficient in the marine atmospheric boundary layer. *Journal of Physical Oceanography*, *40*(10), 2325–2332.

Lenschow, D. H., Savic-Jovcic, V., & Stevens, B. (2007). Divergence and vorticity from aircraft air motion measurements. *Journal of Atmospheric and Oceanic Technology*, *24*(12), 2062–2072.

Lilly, D. (1968). Models of cloud-topped mixed layers under a strong inversion. *Quarterly Journal of the Royal Meteorological Society*, *94*, 292–309.

Marshall, J., & Plumb, R. A. (2016). *Atmosphere, ocean and climate dynamics: An introductory text* (Vol. 21). Cambridge, MA: Academic Press.

Moon, I.-J., Ginis, I., Hara, T., & Thomas, B. (2007). A physics-based parameterization of air–sea momentum flux at high wind speeds and its impact on hurricane intensity predictions. *Monthly Weather Review*, *135*(8), 2869–2878.

Sandu, I., Beljaars, A., Bechtold, P., Mauritsen, T., & Balsamo, G. (2013). Why is it so difficult to represent stably stratified conditions in numerical weather prediction (NWP) models. *Journal of Advances in Modeling Earth Systems*, *5*, 117–133. https://doi.org/10.1002/jame.20013

Schröter, J. S., Moene, A. F., & Holtslag, A. A. (2013). Convective boundary layer wind dynamics and inertial oscillations: The influence of surface stress. *Quarterly Journal of the Royal Meteorological Society*, *139*(676), 1694–1711.

Seibert, P., Beyrich, F., Gryning, S.-E., Joffre, S., Rasmussen, A., & Tercier, P. (2000). Review and intercomparison of operational methods for the determination of the mixing height. *Atmospheric Environment*, *34*(7), 1001–1027.

Stevens, B. (2006). Bulk boundary-layer concepts for simplified models of tropical dynamics. *Theoretical and Computational Fluid Dynamics*, *20*, 279–304. https://doi.org/10.1007/s00162-006-0032-z

Stevens, B., Duan, J., McWilliams, J. C., Münnich, M., & Neelin, J. D. (2002). Entrainment, Rayleigh friction, and boundary layer winds over the tropical Pacific. *Journal of Climate*, *15*(1), 30–44.

Svensson, G., & Holtslag, A. A. (2009). Analysis of model results for the turning of the wind and related momentum fluxes in the stable boundary layer. *Boundary-Layer Meteorology*, *132*(2), 261–277.

Tan, Z.-M. (2001). An approximate analytical solution for the baroclinic and variable eddy diffusivity semi-geostrophic Ekman boundary layer. *Boundary-Layer Meteorology*, *98*(3), 361–385.

Van der Dussen, J. J., de Roode, S. R., & Siebesma, A. P. (2016). How large-scale subsidence affects stratocumulus transitions. *Atmospheric Chemistry and Physics*, *16*, 691–701.

Wu, R., & Blumen, W. (1982). An analysis of Ekman boundary layer dynamics incorporating the geostrophic momentum approximation. *Journal of the Atmospheric Sciences*, *39*(8), 1774–1782.

Young, G., Connolly, P. J., Dearden, C., & Choularton, T. W. (2018). Relating large-scale subsidence to convection development in Arctic mixed-phase marine stratocumulus. *Atmospheric Chemistry and Physics*, *18*, 1475–1494.

Zhang, Y., Stevens, B., Medeiros, B., & Ghil, M. (2009). Low-cloud fraction, lower-tropospheric stability, and large-scale divergence. *Journal of Climate*, *22*(18), 4827–4844.